Life Sciences 229 (2019) 261–276

Contents lists available at ScienceDirect

Life Sciences

journal homepage: www.elsevier.com/locate/lifescie

FGF-2 targets sclerostin in bone and myostatin in skeletal muscle to mitigate the deleterious effects of glucocorticoid on musculoskeletal degradation☆

Sulekha Adhikary, Dharmendra Choudhary, Ashish Kumar Tripathi, Anirudha Karvande, Naseer Ahmad, Priyanka Kothari, Ritu Trivedi*

Division of Endocrinology, CSIR-Central Drug Research Institute, Lucknow 226031, India

ARTICLE INFO

Keywords:
FGF-2
Wnt/β-catenin
Glucocorticoid-induced osteoporosis
Skeletal muscle atrophy
Myostatin

ABSTRACT

Aim: Myokines are associated with regulation of bone and muscle mass. However, limited information is available regarding the impact of myokines on glucocorticoid (GC) mediated adverse effects on the musculoskeletal system. This study investigates the role of myokine fibroblast growth factor-2 (FGF-2) in regulating GC-induced deleterious effects on bone and skeletal muscle.

Methods: Primary osteoblast cells and C2C12 myoblast cell line were treated with FGF-2 and then exposed to dexamethasone (GC). FGF-2 mediated attenuation of the inhibitory effect of GC on osteoblast and myoblast differentiation and muscle atrophy was assessed through quantitative PCR and western blot analysis. Further, FGF-2 was administered subcutaneously to dexamethasone treated mice to collect bone and skeletal muscle tissue for in vivo analysis of bone microarchitecture, mechanical strength, histomorphometry and for histological alterations in treated tissue samples.

Key findings: FGF-2 abrogated the dexamethasone induced inhibitory effect on osteoblast differentiation by modulating BMP-2 pathway and inhibiting Wnt antagonist sclerostin. Further, dexamethasone induced atrophy in C2C12 cells was mitigated by FGF-2 as evident from down regulation of atrogenes expression. FGF-2 prevented GC-induced impairment of mineral density, biomechanical strength, trabecular bone volume, cortical thickness and bone formation rate in mice. Additionally, skeletal muscle tissue from GC treated mice displayed weak myostatin immunostaining and reduced expression of atrogenes following FGF-2 treatment.

Significance: FGF-2 mitigated GC induced effects through inhibition of sclerostin and myostatin expression in bone and muscle respectively. Taken together, this study exhibited the role of exogenous FGF-2 in sustaining osteoblastogenesis and inhibiting muscle atrophy in presence of glucocorticoid.

1. Introduction

Glucocorticoid (GC) based medications have potent anti-inflammatory effects and are widely used to treat chronic inflammatory conditions such as inflammatory bowel disease, systemic lupus, rheumatoid arthritis and chronic obstructive pulmonary disease [1–3]. However, rapid bone loss and skeletal muscle atrophy is reported due to long term glucocorticoid treatment thus leading to osteopenia, increased fracture risk, fatigue, muscle weakness and impaired wound healing [4,5]. The underlying mechanism behind the progressive deterioration of bone and skeletal muscle is inhibition of anabolic process and transient stimulation of catabolic processes. GCs leads to impaired bone formation by inhibiting the Wnt/β-catenin [6–8] and BMP mediated pathways [9,10] for osteoblast differentiation. It increases the expression of Wnt signaling antagonists (sclerostin and Dkk-1) thus suppressing Wnt mediated osteoblastogenesis [11–13]. Muscle proteolysis associated with GCs is mediated through the increased expression of several atrogenes ('genes involved in atrophy'), such as atrogin-1 and MuRF-1; these are ubiquitin ligases involved in the targeting of protein to be degraded by the proteasome machinery [14–16]. These atrogenes in turn are stimulated by increased level of myostatin, a growth factor which inhibits muscle mass development by down-regulating the proliferation pathway through active FOXO, apparently leading to expression of atrogenes [15,17–19].

☆ Research funding: University Grant Commission (UGC), Council of Scientific and Industrial Research (CSIR), Indian Council of Medical Research (ICMR), Government of India.

* Corresponding author at: Division of Endocrinology, CSIR-Central Drug Research Institute, B.S. 10/1, Sector 10, Jankipuram Extension, Sitapur Road, Lucknow 226031, Uttar Pradesh, India.

E-mail address: ID-ritu_trivedi@cdri.res.in (R. Trivedi).

https://doi.org/10.1016/j.lfs.2019.05.022
Received 18 March 2019; Received in revised form 3 May 2019; Accepted 9 May 2019
Available online 10 May 2019

Bone and skeletal muscle are anatomically and functionally connected. The maintenance of both bone and muscle mass is tightly coupled in both healthy and in state of metabolic abnormality. The musculoskeletal system is influenced by common signaling networks triggered by cytokines, growth factors or myokines under different metabolic conditions [20,21]. Muscle derived factors are known to influence bone metabolism in both positive and negative manner and vice versa [22]. Moreover, studies have documented that skeletal muscle secreted factor(s) inhibit glucocorticoid and ROS induced cell death of osteocytes [23,24]. The identification of these factors may provide a novel means to avert musculoskeletal degradation induced by GC therapy.

FGF-2 (basic Fibroblast growth factor/bFGF) is a myokine released during muscle injury and localized in bone and muscle interface [25]. FGF-2 has been reported in studies to reverse ovariectomy induced osteopenia in rodents by modulating the trabecular and cortical microarchitecture of long bones and vertebra [26,27]. Additionally FGF-2 stimulation of osteoblast differentiation and bone formation occurs through modulation of the Wnt/β-catenin pathway as evident from study on FGF knockout mice [28]. FGF-2 contributes to proliferation and differentiation of skeletal muscle through various MAP kinases [29]. Moreover, FGF-2 inversely modulates the expression of myostatin in skeletal muscle cells [30]. Myostatin deletion has been reported to inhibit muscle atrophy in glucocorticoid-treated mice, by blunting the glucocorticoid-induced enhanced proteolysis [18].

In this context, the pathophysiology of glucocorticoid induced osteo-sarcopenia can be associated with inhibition of Wnt/β-beta catenin signaling in bone and increased expression of myostatin in skeletal muscle. Thus it was hypothesized that secretory factors exhibiting a constructive effect on both the tissue can be efficient from the therapeutic point of view. In this study, we have investigated whether FGF-2 plays a role in modulating GC signaling in bone-muscle crosstalk and alleviate the GC induced musculoskeletal deterioration.

2. Materials and methods

2.1. Reagents and chemicals

Cell culture medium and supplements were purchased from Invitrogen (Carlsbad, CA, USA). All fine chemicals were purchased from Sigma-Aldrich (St Louis, MO, USA). Human PTH (1–34) and FGF-2 was purchased from Calbiochem (EMD Millipore Corporation, Billerica, MA, USA). ELISA kits were purchased from Qayee Bio-Technology Co. Ltd., Shanghai, China, ECL kit from GE Healthcare Bio-Sciences (Pittsburgh, PA, USA). Antibodies were procured from Abcam (Cambridge Science Park, Cambridge, UK) and Cell Signaling Technologies (Danver, MA).

2.2. Cell culture and treatment

Calvarial bone cells were isolated from 1 to 2 days old mice pups. The dissected calvariae were cleaned by removing loosely adherent fibrous tissue tags and blood vessels and subjected to sequential enzymatic digestion [31], Cells collected after digestion was plated in α-Minimum Essential Medium (α -MEM), supplemented with 15% fetal bovine serum (FBS) and antibiotics. To assess the role of FGF-2 in abrogating dexamethasone induced inhibition of osteoblastogenesis cells were kept under serum starvation overnight, and then pre-treated with vehicle and dexamethasone (1 μM). After 30 mins cells were treated with FGF-2 ($20\,ng.ml^{-1}$) for 6 h then differentiated in osteogenic medium supplemented with β- glycerophophate (10 mM) and ascorbic acid ($50\,g.ml^{-1}$) for 24 h.

C2C12 cells (American Type Culture Collection, Manassas, VA, USA) were cultured in DMEM, supplemented with 10% FBS and antibiotics. Cells were treated with FGF-2 for 6 h after overnight serum withdrawal and the medium was replaced with DMEM containing 2% horse serum to induce myoblast fusion and differentiation for 48 h. To induce atrophy cell were treated with dexamethasone (1 μM) after plating.

2.3. Bone marrow culture

BMCs from adult mice were isolated and cultures prepared according to a previously published protocol [32]. Briefly, the femora were excised aseptically and marrow flushed out in culture medium consisting of α-MEM, supplemented with 15% FBS, 10^{-7} M dexamethasone, 50 g/ml ascorbic acid, and 10 mM β-glycerophosphate. Cell suspension of released BMCs was collected and plated (2×10^6 cells/well of 12-well plate) for mineralization assay. Cells were cultured with/without dexamethasone (1 μM) and FGF-2 (transient treatment of 6 h) for 21 (mineralization) days. After 21 days, the attached cells were fixed and stained with 40 mM Alizarin Red−S, which stains areas rich in nascent calcium. The stain was quantified and O.D taken at 405 nm [31].

Further, to investigate the ex vivo effect of treatment on osteoblast pool in bone marrow, osteoblast cells were differentiated from bone marrow of different animal treatment groups and analyzed for RUNX-2 expression through qPCR [33].

2.4. Cell proliferation assay

Cell proliferation was studied by using BrdU incorporation assay (Roche Applied Sciences, Branford, CT, USA). Cells were subjected to FGF-2 treatment (as mentioned earlier), followed by incubation in proliferation medium with/without dexamethasone and labeled with BrdU. Cells stained with BrdU were detected by BrdU antibody according to the protocol given in kit and O.D. (optical density) measured at 450 nm.

2.5. Immunofluorescence in calvarial osteoblasts to detect nuclear translocation

Calvarial osteoblasts cell were incubated in medium with/without dexamethasone (1 μM) and FGF-2 ($20\,ng.ml^{-1}$) and were grown in for 24 h. For immunocytochemistry, cells were fixed with 4% formaldehyde and permeabilized with 0.1% triton X-100. Cells were incubated in primary antibody for phospho-β-catenin overnight, followed by Alexa Flour 488 tagged secondary antibody for 1 h. Thereafter, cells were stained with 4,6-diamidino-2-phenylindole (DAPI) for 5 min and embedded in ProLong™ Gold Antifade Mountant medium. Images were captured using fluorescent microscope (Eclipse 80i, Nikon, Tokyo, Japan), with the aid of appropriate filter (excitation 495 nm and emission 519 nm) [34].

2.6. Quantitative RT-PCR and western blotting

RNA was isolated using trizol method from cells subjected to different treatments. Revert Aid cDNA Synthesis Kit (Fermentas, Austin, TX) was used, and cDNA were amplified with SYBR green-based real-time PCR reactions using a standard protocol (Roche Diagnostics). Each sample was assayed in a 15 μL reaction in triplicate under same conditions (initial melt at 94 °C for 3 min followed by 40 cycles of 94 °C for 30 s, 48 °C for 30 s, 72 °C for 44 s with final extension for 10 min at 72 °C). The data were analyzed using GAPDH (osteoblast specific gene) and β-actin (muscle specific gene) as the internal control with the cycle threshold $2^{(-\Delta\Delta CT)}$ method. The fold change was calculated as $2^{(-\Delta\Delta Ct)}$, where $\Delta Ct = Cttarget\ gene - CtGAPDH$ or β-actin and $\Delta\Delta Ct = \Delta Cttreatment - \Delta Ctvehicle$.

Western blot analysis was performed as described previously [34]. Briefly, 30 μg protein were resolved by 8%–12% SDS PAGE, transferred to PVDF membranes (Millipore; Billerica, MA) and were detected using chemiluminescent HRP substrate (Millipore) based detection system in Imager Quant LAS 4010 Chemidoc (GE Healthcare, Little Chalfont, UK).

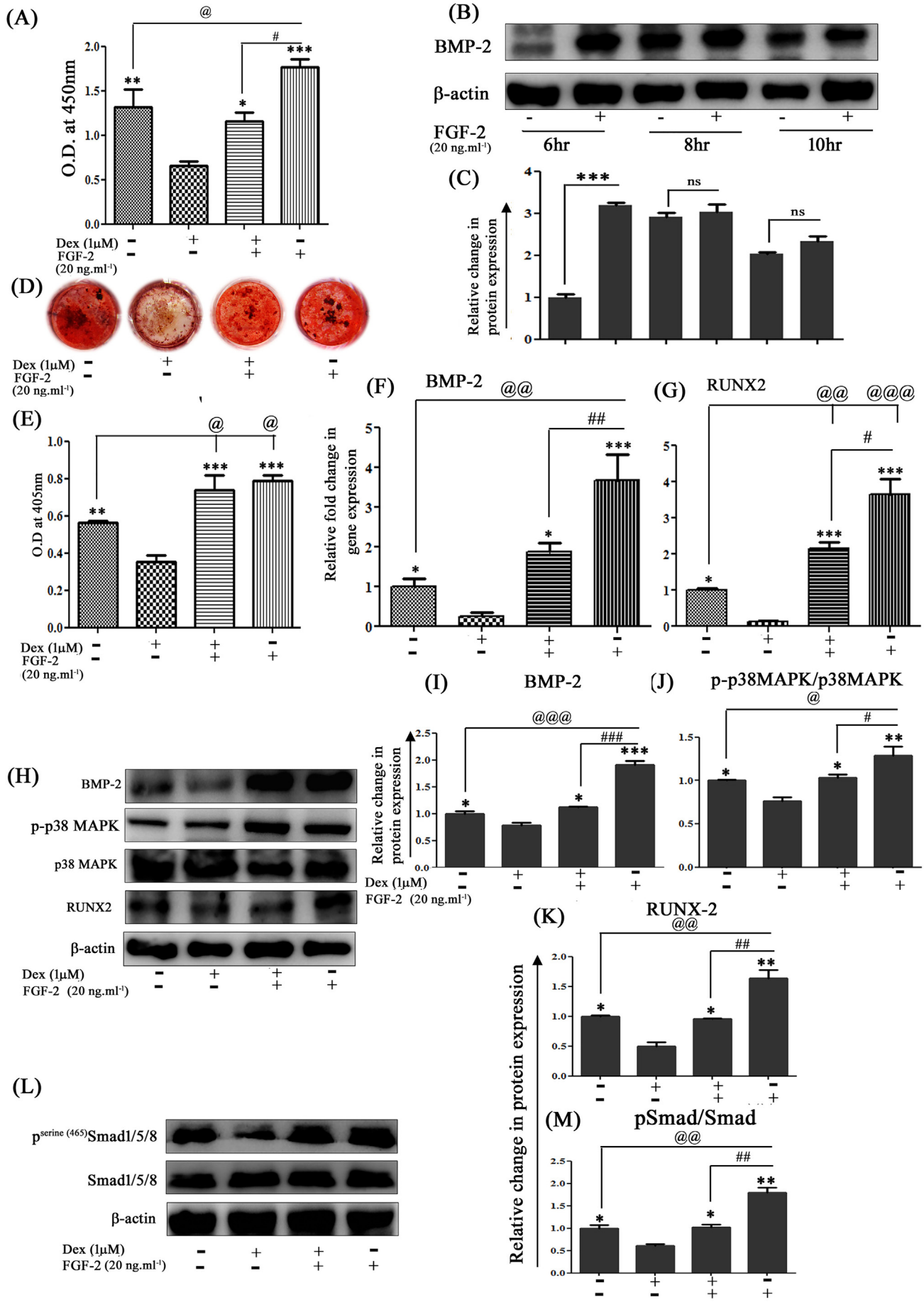

(caption on next page)

Fig. 1. (A) Proliferation of osteoblast cells as assessed by BrdU assay. (B–C) Representative image and densitometry analysis of western blots depicting BMP-2 expression under transient FGF-2 treatment in osteoblast cells. (D–E) Representative images and quantification of alizarin stained cells treated with FGF-2 and dexamethasone. Quantitative PCR analysis depicted relative fold change in gene expression of (F) BMP-2, (G) RUNX2. Data were expressed after normalization with the housekeeping gene GAPDH. Western blot of (H) BMP-2 (pAb ab14933-Abcam; 1:1000), phospho p38 MAPK (pAb 9211S-Cell Signaling Technology; 1:1000), p38 MAPK (pAb 9212S-Cell Signaling Technology; 1:1000), RUNX-2 (mAb ab76956-Abcam; 1:1000) and quantitative analysis depicted change in protein expression of (I) BMP-2, (J) phospho p38 MAPK/p38 MAPK ratio, (K) RUNX2. (L) Representative western blot images and quantitative analysis depicted change in protein expression of (M) phosphor-smad 1/5/8 (mAb 9516S-Cell Signaling Technology; 1:1000) and smad 1/5/8 (pAb sc6031-R Santa Cruz Biotechnology; 1:500) in osteoblast cells treated with FGF-2 and dexamethasone. β-actin (sc-47778 Santa Cruz Biotechnology; 1:500) was taken as a loading control. Secondary antibodies (either anti-rabbit or anti-mouse; 1:10,000) were HRP conjugated (Sigma-Aldrich). Results were obtained from three independent experiments performed in triplicate and are expressed as Mean ± SEM. $^{*}p < 0.05$, $^{**}p < 0.01$ $^{***}p < 0.001$ versus dex; $^{@}p < 0.05$, $^{@@}p < 0.01$ $^{@@@}p < 0.001$ versus control; $^{\#}p < 0.05$, $^{\#\#}p < 0.01$ $^{\#\#\#}p < 0.001$ versus FGF-2 + dex treated group. Dex, dexamethasone; FGF-2, fibroblast growth factor-2.

Blots were stripped and reused whenever possible.

2.7. Induction of glucocorticoid-induced bone loss in mice

Study was implemented in accordance with current legislation of animal experiments (Institutional Animal Ethical Committee at Central Drug Research Institute, Lucknow). 12 weeks old male BALB/c mice ($n = 40$) (22–25 g each) were obtained from the National Laboratory Animal Centre, CSIR-CDRI. Animals were maintained under controlled room temperature (22 ± 2 °C) and humidity (50 ± 5%) with a 12:12 h light/dark cycle and fed with commercially available normal pellet diet and water ad libitum throughout the study. After acclimatization animals were randomly divided into four groups ($n = 10$ mice/group), control (treated with saline), dexamethasone (treated with 5 $mg.kg^{-1}.d^{-1}$ s.c), dexamethasone + FGF-2 (100 $\mu g.kg^{-1}.d^{-1}$ s.c) and dexamethasone + PTH (20 $\mu g.kg^{-1}.d^{-1}$ s.c. thrice a week). To trace dynamic bone formation, each mouse was given tetracycline and calcein intraperitoneally (25 $mg.kg^{-1}$) 15 and 3 days before sacrifice. After a total of 4 weeks, mice were killed by asphyxiation and bones collected for further study.

2.8. Microcomputed tomography (μCT)

Micro-computed tomography of excised bones was conducted by using SkyScan 1076 CT-scanner (Aartselaar, Belgium) using previously published protocol [33]. Briefly, excised bones were scanned at 50 kV, 200 mA and resolution of 9 μm/pixel. Cross sectional reconstruction was made using Nrecon software based on modified Feldkamp algorithm. To analyze trabecular region, 100 slices for region of interest (ROI) were selected using CTAn software below the growth plate. For cortical bone analysis 100 consecutive image slides were selected at mid-diaphysis region. Quantification was done applying Batman software and BMD calculated from the VOI (volume of interest) made for trabecular region using hydroxyapatite phantom rods of 4 mm diameter as standards.

2.9. Bone strength testing and dynamic histomorphometry

To assess biomechanical properties, femurs in each group were subjected to three-point bending using a bone strength tester model TK 252C (Muromachi Kikai Co. Ltd., Tokyo, Japan). Briefly, the bone was placed on two support points, and a third (loading) point applied a downward force (1 $mm.s^{-1}$) at the mid-diaphysis region. For femur, the anterior surface was faced down, so the posterior aspect of the femoral condyles faced up. Failure typically occurred at/near loading site resulting in a crack formation on the anterior surface propagating across the bone to the posterior surface [35]. The load–displacement curves generated were used to calculate the ultimate load, stiffness and energy to failure.

For dynamic histomorphometric measurements cross sections (50 μm) of undecalcified femur diaphysis were obtained using an IsoMet Low Speed Bone Cutter (Buehler, Lake Bluff, IL, USA) [36]. Images were captured using Leica-Qwin software (Leica Microsystems, Buffalo Grove, IL) and single labeled surface (sLS), double labeled surface (dLS), and interlabeled thickness (IrLTh) were measured. These data were used to calculate mineralizing surface/bone surface (MS/BS), mineral apposition rate (MAR) and bone formation rate (BFR) as follows: MS/BS = (1/2 sLS + dLS)/BS (%); MAR = IrLTh/12 days ($\mu m.day^{-1}$); BFR/BS = MAR × MS/BS ($\mu m^3.\mu m^{-2}.day^{-1}$) [33].

2.10. Quantitative realtime PCR of bone and muscle

Bones and skeletal muscle were excised during autopsy, cleaned and collected in RNA later. For RNA isolation the bones and skeletal muscle were separately crushed in liquid nitrogen and collected in Trizol (Invitrogen). RNA isolation procedure was performed according to the manufacturer's protocol. 500 ng of RNA was used for cDNA synthesis with Revert Aid cDNA synthesis kit (Fermentas, Austin, TX). Real Time PCR (qPCR) was performed using the Light Cycler 480 (Roche Molecular Biochemical's, USA) real time PCR machine with SYBR green (PureGene, USA) for quantitative determination of relative expression of bone and muscle specific genes. GAPDH was used as the internal control in this study. Primer sequences are summarized in Supplementary Table 1 [37].

2.11. Histological analysis of bone and muscle

Undecalcified distal femur metaphyseal bone was embedded in methyl methacrylate for polymerization. 5 μm longitudinal sections were cut at room temperature with a Leica RM2265 semi-automatic microtome (Wetzlar, Germany) equipped with a TC-65 profile knife with a tungsten carbide cutting edge and stained with Goldner's trichrome. Thereafter, bone volume (BV/TV), trabecular number (Tb.N) were measured using Bioquant Osteo Software (Bioquant Image Analysis, Nashville, TN, USA). For muscle histology gastrocnemius muscles were carefully dissected and stored in chilled PBS for 4–8 h. Tissues were brought to room temperature, rehydrated in PBS and fixed in 10% formalin and kept in 70% isopropanol for embedding into parrafin. 5 μm sections were cut on a Leica microtome and transferred onto poly-L lysine coated slides. Later, sections were de-paraffinzed and rehydrated in serial changes of isopropanol and stained with hematoxylin and eosin, mounted with DPX (Sigma) and were examined under microscope [37].

2.12. Immunohistochemical staining of bone and muscle tissues

The expression of the indicated proteins was visualized in paraffin-embedded bone and skeletal muscle sections from treated animals. Briefly, sections were de-paraffinized, rehydrated through xylene and a series of graded ethanol solutions. Endogenous peroxidase was blocked by incubating sections with 0.3% H_2O_2 in PBS for 15 min. Sections were then washed 3 times in PBS. Blocking was with 10% rabbit serum in PBS for 1 h at room temperature and then incubated with rabbit polyclonal anti-sclerostin antibody for bone; rabbit polyclonal anti-myostatin antibody for muscles. Sections were then incubated with the corresponding biotinylated secondary antibody followed by avidin conjugated peroxidase (Vectastain Elite ABC Kit; Vectora Laboratories). Color was developed with a diaminobenzidine substrate chromogen

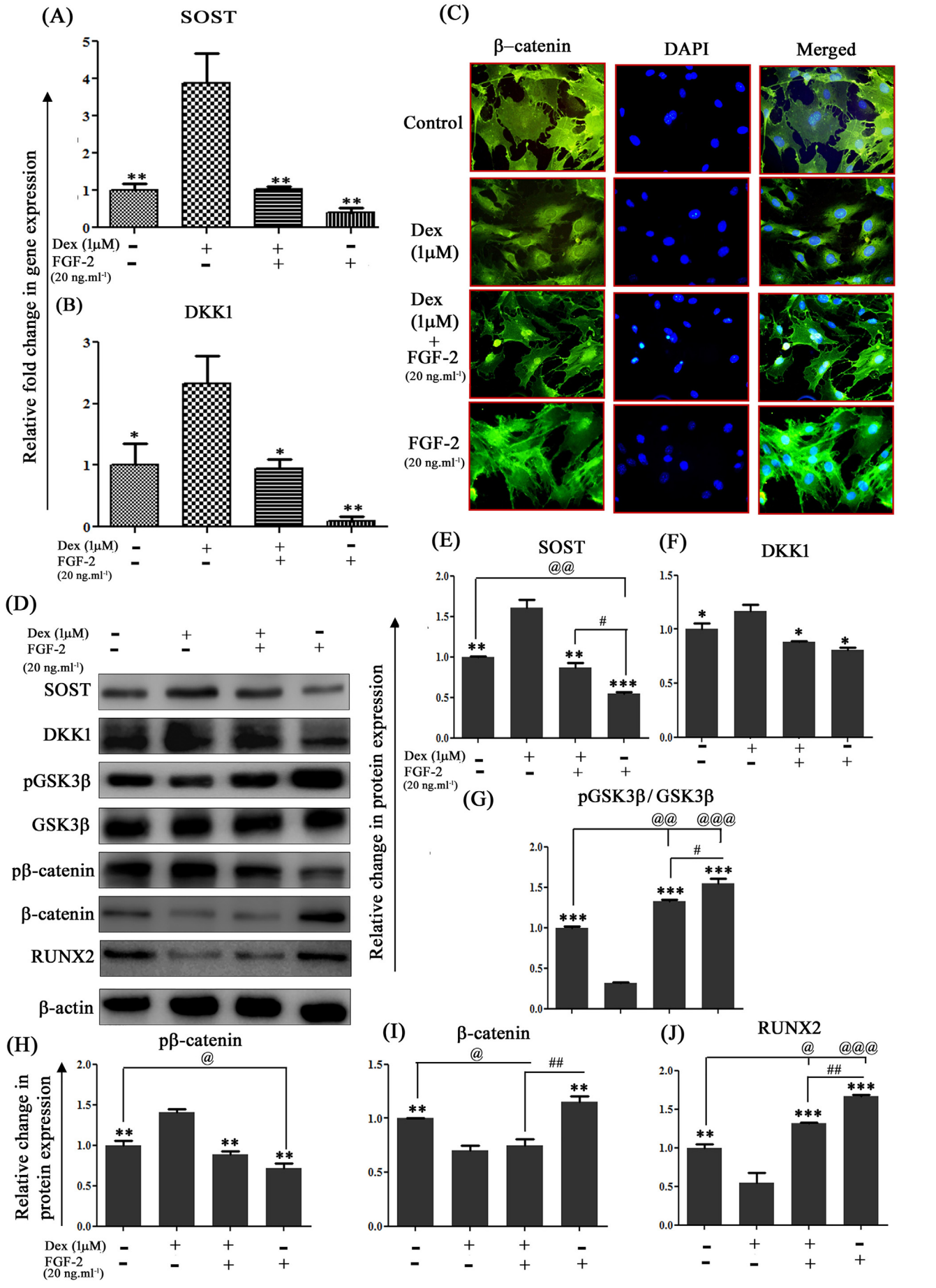

(caption on next page)

Fig. 2. FGF-2 mitigated dexamethasone induced inhibition of Wnt/β-catenin signaling in osteoblasts. Relative fold change in gene expression compared to control group of (A) SOST, (B) DKK-1 as analyzed by realtime qPCR. Data is expressed after normalization with the housekeeping gene GAPDH. (C) FGF-2 alleviates the dexamethasone induced inhibition of β-catenin nuclear translocation in osteoblast cells. Representative photomicrograph of sub-cellular localization of β-catenin was determined by immunofluorescence (magnification 40×) under control and treatment conditions from three independent experiments ($n = 3$). Representative images of western blot (D) and densitometry analysis depicting the change in protein expression of (E) SOST (pAb ab63097-Abcam;1:1000), (F) DKK-1 (mAb sc-374,574 Santa Cruz Biotechnology; 1:500), (G) pGSK3β (mAb 9322S-Cell Signaling Technology; 1:1000)/GSK3β (mAb 12456S- Cell Signaling Technology; 1:1000) ratio, (H) pβ-catenin (pAb 9561S-Cell Signaling Technology; 1:1000), (I) β-catenin (mAb 9582S-Cell Signaling technology; 1:1000), (J) RUNX-2 (mAb ab76956-Abcam; 1:1000) in osteoblast cells treated with FGF-2 and dexamethasone. β-actin (sc-47778 Santa Cruz Biotechnology; 1:500) was taken as a loading control. Secondary antibodies (either anti-rabbit or anti-mouse; 1:10,000) were HRP conjugated (Sigma-Aldrich). Results were obtained from three independent experiments performed in triplicate and are expressed as mean ± SEM. $^{*}p < 0.05$, $^{**}p < 0.01$ versus dex; $^{@}p < 0.05$, $^{@@}p < 0.01$, $^{@@@}p < 0.001$ versus control; $^{\#}p < 0.05$, $^{\#\#}p < 0.01$ versus FGF-2 + dex treated group. Dex, dexamethasone; FGF-2, fibroblast growth factor-2.

system (Dako Corp.). Cells expressing the protein of interest were stained brown [38,39]. All the immuno-stained sections were scored independently in a blinded manner, based on the H-score method, which reflected the staining intensity of positively stained cells. 10 fields were chosen randomly and the staining intensity of cells were scored as 0, 1, 2 and 3 corresponding to the zero, weak, intermediate and strong staining, respectively. The H-score was calculated following the formula: (% of cells stained at intensity category 1 × 1) + (% of cells stained at intensity category 2 × 2) + (% of cells stained at intensity category 3 × 3). H-scores varied from 0 to 300 where 300 represented 100% of cells strongly stained (3+) [40].

2.13. Serum markers of bone formation and resorption

Bone formation marker osteocalcin (OCN), resorption markers Carboxy-terminal collagen crosslinks (CTX-1) and sclerostin (SOST) were determined by enzyme-linked immunosorbent assay kits following the manufacturer's protocols from serum collected from individual mice [33] at the end of treatment regimen. Likewise, myostatin level was measured to detect muscle atrophy.

2.14. Statistical analysis

Data are expressed as mean ± SEM unless otherwise indicated. The data obtained from experiments were subjected to one-way ANOVA followed by Newman Keul's multiple comparison test of significance using GraphPad prism 5.

3. Results

3.1. FGF-2 abrogated dexamethasone-attenuated osteogenic activities in-vitro

Dexamethasone impairment of osteoblasts proliferation and differentiation was attenuated by FGF-2 treatment. The proliferative effect of FGF-2 on dexamethasone treated osteoblasts cells were analyzed by BrdU assay. FGF-2 resulted in increased BrdU incorporation in osteoblast cells ($p < 0.05$) treated with dexamethasone thus mitigating the anti-proliferative effect (Fig. 1A). Impact of FGF-2 on osteoblast differentiation was evident from the ~3 fold ($p < 0.001$) increased expression of BMP-2 (representative western blot image and densitometry analysis (Fig. 1B and C)) after transient treatment with FGF-2 (20 $ng.ml^{-1}$) for 6 h, followed by change to osteogenic media for 24 h. Osteoblasts derived from bone marrow cells exhibited increased mineralization with FGF-2 treatment in the presence of dexamethasone as indicated by increased nodule formation (Fig. 1D) and quantification ($p < 0.001$) (Fig. 1E) of Alizarin Red-S stained culture. Dexamethasone-induced transcriptional inhibition of bone morphogenetic protein −2 (BMP-2) (Fig. 1F) and runt-related transcription factor-2 (RUNX2) (Fig. 1G) ($p < 0.05$) expression was antagonized by treatment with FGF-2 as depicted by ~2 fold ($p < 0.05$; $p < 0.001$) stimulation of gene expression in dexamethasone-exposed cells. Osteocalcin (OCN), the matrix protein (Supplementary Fig. 1A) was elevated more than ~2 folds ($p < 0.05$) compared to control whereas, collagen-1 (COL1) (Supplementary Fig. 1B) was equivalent to control after stimulation with FGF-2. FGF-2 attenuated dexamethasone-induced inhibition of BMP-2, phosphorylated p38 MAPK (Fig. 1H) and smad1/5/8 (Fig. 1L) protein expressions apparently leading to increased RUNX-2 (Fig. 1H) levels in dexamethasone exposed cells. Overall, results suggested that transient treatment with FGF-2 antagonized the inhibitory effect of dexamethasone on osteoblast differentiation by up-regulating BMP-2 ($p < 0.05$) through smad1/5/8 ($p < 0.05$) and p38 MAPK phosphorylation ($p < 0.05$).

3.2. FGF-2 via Sost modulated Wnt/β-catenin signaling to stimulate survival of dexamethasone treated osteoblast cells

We further elucidated the potential mechanisms by which FGF-2 alleviates dexamethasone-mediated inhibition of Wnt/β-catenin signaling. Realtime PCR results demonstrated that the increased expression of Wnt antagonists Sost ($p < 0.01$) (Fig. 2A) and Dkk1 ($p < 0.05$) (Fig. 2B) was abrogated with a brief stimulation of FGF-2 to dexamethasone exposed osteoblasts cells. However, surprisingly, FGF-2 failed to increase the expression of Wnt10b ligand (Supplementary Fig. 1C) which was down-regulated under the influence of dexamethasone. Further, FGF-2 resulted in β-catenin translocation to nucleus in dexamethasone exposed cells (Fig. 2C) exhibited by intra-nuclear staining of β-catenin, thus reflecting activated Wnt/β-catenin signaling. Immunoblotting results showed that dexamethasone markedly increased Sost and Dkk1 secretion, which apparently led to β-catenin phosphorylation by attenuating the inhibitory GSK3β (Ser^{9}) phosphorylation (Fig. 2D), indicating the inhibitory effect on Wnt/β-catenin pathway. FGF-2 antagonized the effect of dexamethasone as demonstrated in immunoblots by declining the expression of Wnt inhibitors Sost ($p < 0.01$), Dkk1 ($p < 0.05$) and stimulating phosphorylation of GSK3β (Ser^{9}) ($p < 0.001$), apparently decreasing phosphorylation of β-catenin ($p < 0.01$) to facilitate β-catenin trafficking in the nucleus thus leading to enhanced RUNX-2 ($p < 0.001$) expression. Overall, the data implied that FGF-2 stimulated Wnt/β-catenin signaling in the presence of dexamethasone, thus sustaining the expression of RUNX-2 in osteoblasts.

3.3. Effects of dexamethasone on muscle specific atrophy genes in C2C12 myoblast cells

To investigate the effect of FGF-2 on dexamethasone-induced muscle atrophy, C2C12 myoblast cells were used to induce atrophy in vitro. Myostatin (Fig. 3A) was down-regulated ($p < 0.001$) and myogenin (Fig. 3C) stimulated ($p < 0.01$) in differentiating myoblast cells under the influence of FGF-2 as evident from western blot analysis. Dexamethasone-induced muscle atrophy was evident from ~3 folds ($p < 0.001$) increase in myostatin (Fig. 3E), atrogin-1 (Fig. 3F) and MuRF-1 (Fig. 3G) gene expression. Concurrent transient FGF-2 treatment for 6 h to dexamethasone exposed differentiating myotubes resulted in mitigating the stimulatory effects on myostatin and atrogenes, and resulted in enhanced myogenin ($p < 0.01$) (Fig. 3H) expression. Additionally, dexamethasone-induced increased FOXO1 level ($p < 0.001$) and reduced MyoD ($p < 0.01$) (Supplementary Fig. 1D,

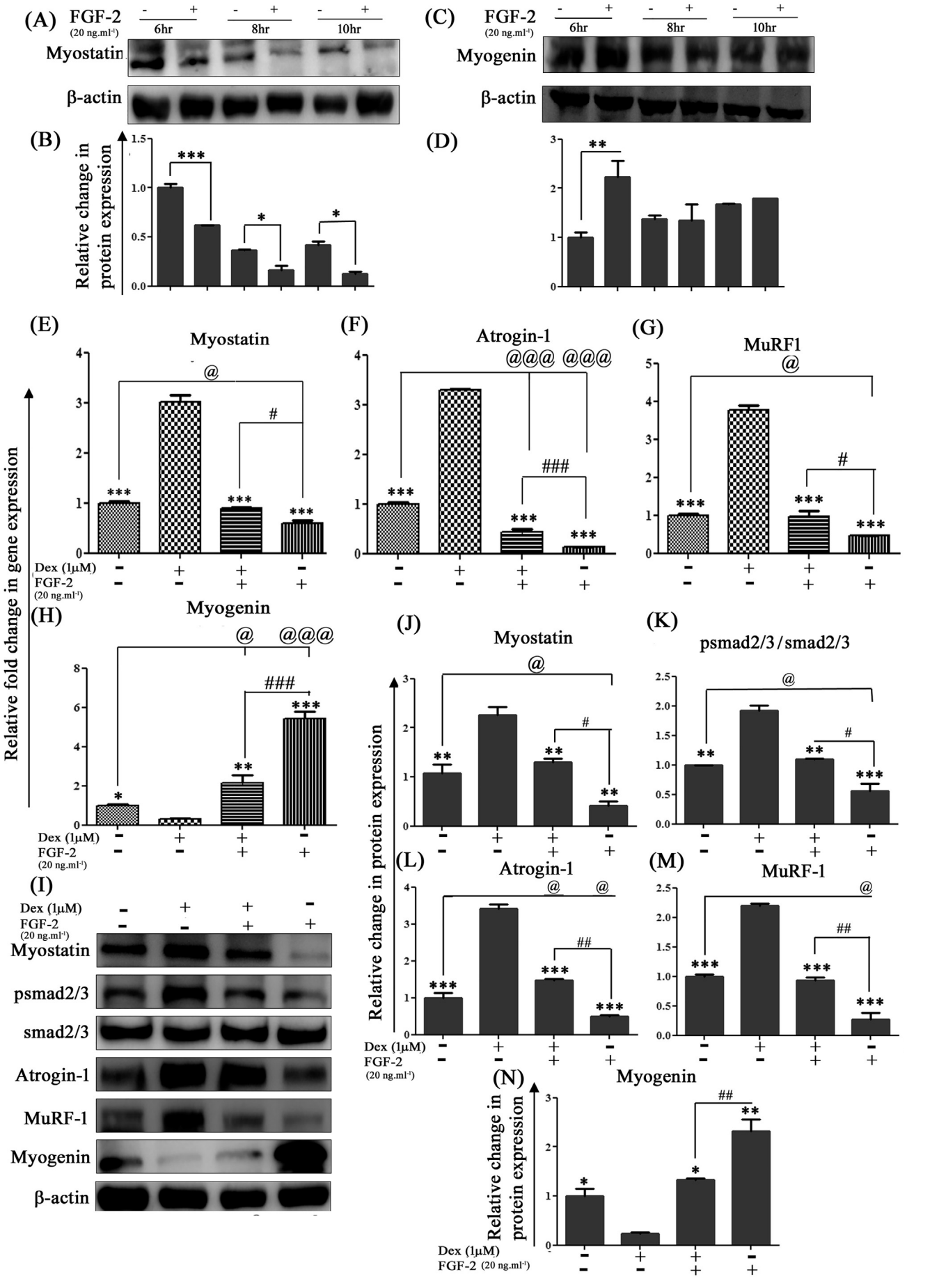

(caption on next page)

Fig. 3. Representative image and quantification of western blots depicting time dependent change in protein expression of (A–B) myostatin (pAb ab203076-Abcam; 1:1000) and (C–D) myogenin (mAb ab1835-Abcam; 1:1000) with FGF-2 treatment in C2C12 cell. FGF-2 inhibited dexamethasone-induced atrophy in differentiated C2C12 myotube cells. Relative fold change in gene expression compared to control group was analyzed by quantitative PCR for (E) Myostatin, (F) Atrogin-1, (G) MuRF-1, (H) Myogenin. Representative images of western blots (I) and densitometry analysis depicting change in protein expression of (J) myostatin (pAb ab203076-Abcam; 1:1000), (K) psmad2/3 (mAb 8828S-Cell Signaling Technology; 1:1000)/smad2/3 (pAb ab217553-Abcam; 1:1000) ratio, (L) atrogin-1 (pAb ab74023-Abcam; 1:1000), (M) MuRF-1 (pAb ab183094-Abcam; 1:1000), (N) myogenin (mAb ab1835-Abcam; 1:1000). Data is expressed as mean ± SEM of three independent experiments $^{*}p < 0.05$, $^{**}p < 0.01$ $^{***}p < 0.001$ versus dex; $^{@}p < 0.05$, $^{@@}p < 0.01$ $^{@@@}p < 0.001$ versus control; $^{\#}p < 0.05$, $^{\#\#}p < 0.01$ $^{\#\#\#}p < 0.001$ versus FGF-2 + dex group. Dex, dexamethasone; FGF-2, fibroblast growth factor-2.

E) levels were restored equivalent to control untreated cells with FGF-2 treatment. Further, incongruent with gene expression, results from western blots analysis of dexamethasone exposed FGF-2 treated cells demonstrated reduced myostatin ($p < 0.01$), atrogin-1 ($p < 0.001$) and muscle ring finger motif-1 (MuRF-1) levels ($p < 0.001$) (Fig. 3I). Decreased myostatin signaling was associated with decline in smad2/3 phosphorylation ($p < 0.01$) apparently leading to augmented myogenin ($p < 0.05$) expression further substantiating the fact that FGF-2 inhibited myostatin signaling in dexamethasone induced atrophic condition. Overall, in vitro data revealed that short spurge of FGF-2 treatment led to inhibition of myostatin signaling apparently antagonizing the catabolic effect of dexamethasone on myotubes.

3.4. Effect of FGF-2 on trabecular bone micro-architecture

Measurements of trabecular bone parameters for distal femurs from μCT (representative images Fig. 4A) showed protection from dexamethasone induced bone loss with concurrent administration of FGF-2 for four weeks. Dexamethasone at $5\,mg.kg^{-1}.day^{-1}$ dose decreased bone volume/tissue volume (BV/TV) ($p < 0.001$) (Fig. 4B), bone surface/tissue volume (BS/TV) ($p < 0.01$) (Fig. 4C), trabecular number (Tb.N.) ($p < 0.01$) (Fig. 4D) and connectivity density (Conn.Dn.) ($p < 0.05$) (Fig. 4G) by 37, 32, 30 and 24% respectively compared to control group. FGF-2 treatment improved BV/TV by 34% ($p < 0.01$), similar to PTH that exhibited a rise of 30% ($p < 0.01$) compared to dexamethasone. Increased BV/TV was associated with higher BS/TV (73%) ($p < 0.001$), Tb.N. (52%) ($p < 0.05$) and Conn.Dn. (40%) ($p < 0.05$) in FGF-2 treated group as compared to dexamethasone. The improved trabecular network in FGF-2 group subsequently resulted in 21% reduction in trabecular separation (Tb.Sp) ($p < 0.01$) (Fig. 4E) against dexamethasone group which had a 25% ($p < 0.01$) elevation as compared to control. SMI (Structure model index) defining the arrangement of rods and cones was elevated in dexamethasone animals due to disturbed trabecular network. FGF-2 and PTH treatment resulted in decline in SMI (Fig. 4F) values by 16 ($p < 0.05$) and 20% ($p < 0.01$) respectively.

Similarly, at L5, the dexamethasone-induced loss of trabecular network ($p < 0.01$) (Fig. 4L) was significantly improved by FGF-2, comparable to control group. However, there was no significant change in other parameters. Similar results were obtained from analysis of trabecular region of tibia (Tables 1A). Overall, data revealed that FGF-2 showed a pronounced effect in preventing dexamethasone induced trabecular bone deterioration at the appendicular and axial skeletal sites.

3.5. Effect of FGF-2 on cortical bone micro-architecture

Cortical analysis in mid-femoral diaphyses by μCT exhibited decreased cortical thickness (Ct.Th) ($p < 0.05$) (19%) (Fig. 4H), bone area (B.Ar) (Fig. 4J) and periosteal perimeter (P.Pm) (Fig. 4K) (decline by 29% ($p < 0.001$) for area and 8% ($p < 0.001$) for perimeter) in dexamethasone treated animals compared to control. However, both FGF-2 and PTH groups exhibited cortical parameters comparable to control. The detrimental effect of dexamethasone on cortical surface further translated to 32% ($p < 0.001$) decrease in polar mean moment of inertia (MMI polar) (Fig. 4I). FGF-2 and PTH both mitigated the effect of dexamethasone on MMI polar as exhibited by increase in values by 20% ($p < 0.05$) and 40% ($p < 0.001$) respectively. Cortical tibial analysis also depicted similar outcomes (Tables 1B). Overall, our data revealed that FGF-2 maintained the cortical integrity of bone.

3.6. Effect of FGF-2 on osteogenic gene expression

To confirm the antagonizing effect of FGF-2 on dexamethasone-induced bone deterioration we next investigated the expression of genes involved in bone formation and resorption processes from RNA isolated from entire femoral and tibial region. While dexamethasone resulted in down regulation of bone formation markers RUNX-2 (Fig. 5A), BMP-2 (Fig. 5 B), COL1 and OCN (Supplementary Fig. 2A,B) FGF-2 resulted in stimulation of osteogenic gene expression more than ~2 folds as compared to dexamethasone treated group (RUNX-2, $p < 0.01$; BMP-2, OCN, COL-1, $p < 0.05$)). Likewise, PTH group demonstrated similar effect as FGF-2, being anabolic in its action on dexamethasone induced reduction of gene expression. Additionally, dexamethasone-induced increased RANKL, decreased OPG (Supplementary Fig. 2C, D) levels were reversed by PTH (RANKL, $p < 0.01$; OPG, $p < 0.001$). FGF-2 was proficient in stimulating OPG ($p < 0.001$) expression, while RANKL was down-regulated, but was statistically insignificant to dexamethasone group. In addition, dexamethasone induced stimulation of Wnt inhibitory genes, SOST (Fig. 5C) and DKK1 (Supplementary Fig. 2E) was abrogated in FGF-2 and PTH groups ($p < 0.001$). Overall the results indicated that FGF-2 antagonized the effect of dexamethasone on Wnt inhibitors and sustained osteogenic gene expression.

3.7. Effect of FGF-2 on dynamic histomorphometry

The trabecular and cortical results were further supported by bone histomorphometry data. Histomorphometry analysis of distal femur following Goldner's trichrome (GT) staining (representative images Fig. 5D and E) showed reduced BV/TV (Fig. 5F) ($p < 0.05$) and Tb.N (Fig. 5G) ($p < 0.05$) in dexamethasone animals thus confirming trabecular osteopenia. PTH and FGF-2 both resulted in alleviating this trabecular loss effectively demonstrating increased trabeculae indices. Further, dual calcein labeling (representative images Fig. 5H) revealed that there is a decline in endocortical bone formation in dexamethasone treated animals. 32% and 68% reduction in the rate of mineral apposition (MAR) (Fig. 5I) ($p < 0.05$) and bone formation (BFR) rate (Fig. 5J) ($p < 0.01$) in dexamethasone-induced osteoporotic animals was observed. FGF-2 alleviated dexamethasone induced decrease in bone histomorphometry parameters in cortical femoral diaphysis as evident from the augmentation in MAR and BFR (at the endocortical/periosteal bone surface) in the animals by 54% ($p < 0.01$) and 43% ($p < 0.001$) respectively. The effect of FGF-2 on histomorphometric parameters was however weaker to that observed in PTH treated animals (60 and 70% increase in MAR, BFR; $p < 0.001$).

3.8. Effect of FGF-2 on bone mineral density and strength

We next verified if FGF-2 could mitigate the deteriorating effect of dexamethasone on bone mineral density (BMD) and bone strength parameters (Table 2). Dexamethasone-mediated loss of mineral density

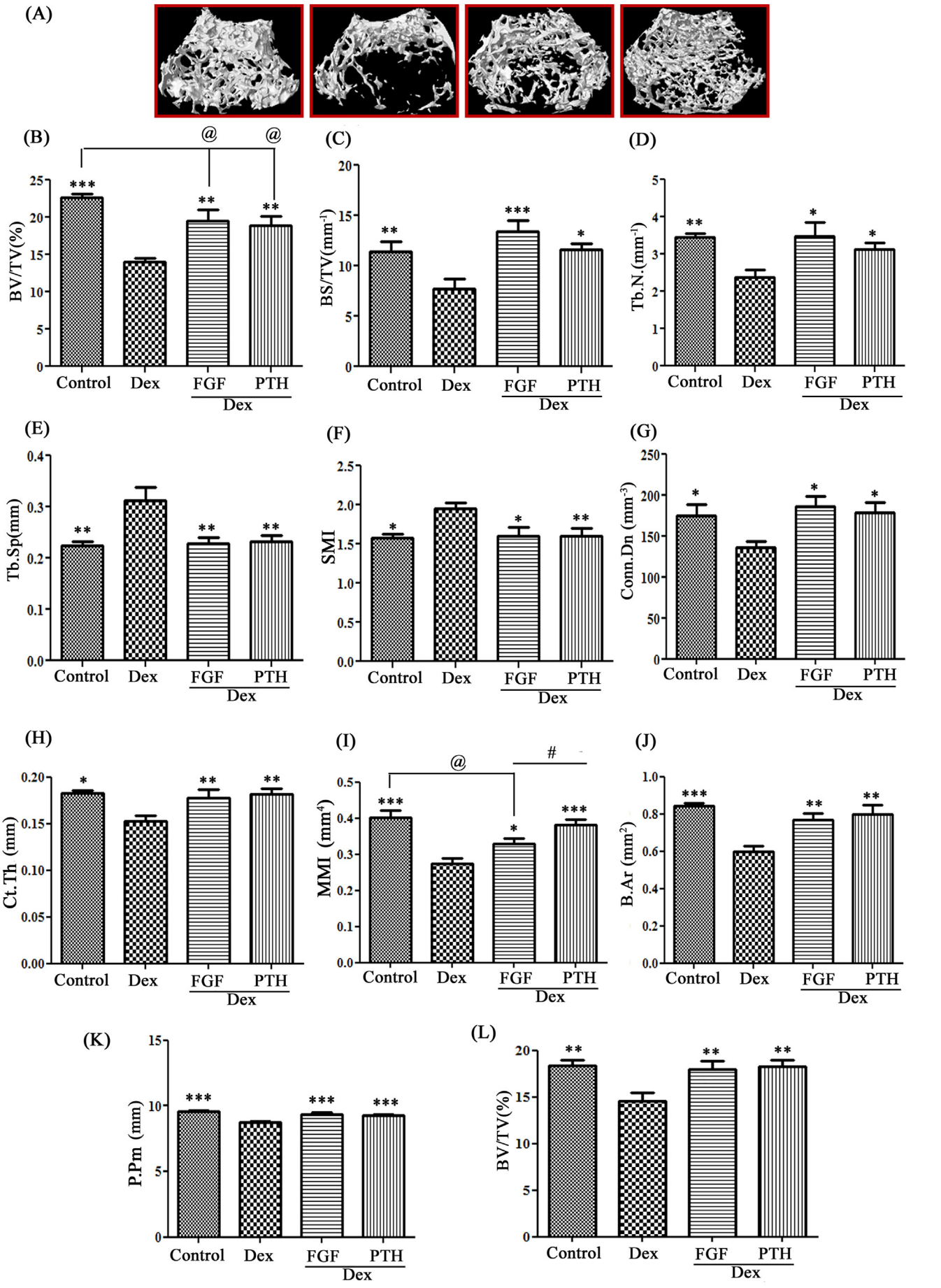

(caption on next page)

Fig. 4. Treatment with FGF-2 mitigated dexamethasone induced bone loss by preventing deterioration of femoral trabecular and cortical microarchitecture. (A) Representative micro-CT images of femoral epiphyseal regions in various experimental groups. Quantification of micro-CT data for various trabecular parameters is presented as follows: (B) bone volume/tissue volume (BV/TV), (C) bone surface/tissue volume (BS/TV), (D) trabecular number (Tb.N), (E) trabecular separation (Tb.Sp), (F) structural model index (SMI), and (G) connectivity density (Conn.Dn.). Quantification of micro-CT data for various cortical parameters is presented as follows: (H) cortical thickness (Ct.Th), (I) mean polar moment of inertia (MMI), (J) bone area (B.Ar), (K) periosteal perimeter (P·Pm) and (L) BV/TV of trabecular L5 vertebra. Results are presented as Mean ± SEM ($n = 10$ mice/group). $^{***}p < 0.001$, $^{**}p < 0.01$, $^{*}p < 0.05$ versus dexamethasone group, $^{\#}p < 0.05$ versus dex + FGF-2 group, $^{@}p < 0.05$ versus control group. Dex, dexamethasone; FGF-2, fibroblast growth factor-2; PTH, parathyroid hormone 1–34.

Table 1
Micro CT analysis of tibial trabecular and cortical microarchitecture.

A Micro-CT parameters for proximal tibial metaphyseal region

Parameters	Control	Dex	Dex + FGF-2	Dex + PTH
BV/TV (%)	20.29 ± 1.1[a]	11.75 ± 0.83	16.9 ± 1.12[b,z]	16.36 ± 1.32[b,z]
BS/TV (mm^{-1})	13.64 ± 1.03[a]	7.58 ± 0.49	11.7 ± 0.89[b]	11.83 ± 0.66[b]
Tb.N (mm^{-1})	3.89 ± 0.25[a]	2.38 ± 0.2	3.36 ± 0.18[b]	3.81 ± 0.32[a]
Tb.Sp (mm)	0.20 ± 0.016[b]	0.29 ± 0.0226	0.23 ± 0.021[c]	0.22 ± 0.008[c]
SMI	1.68 ± 0.061[b]	2.14 ± 0.031	1.68 ± 0.115[c]	1.63 ± 0.16[b]
Conn.D (mm^{-3})	208.35 ± 15.0[a]	80.48 ± 7.75	152.28 ± 25.09[b]	185.69 ± 14.63[a]

B Micro-CT parameters for tibial diaphyseal region

Parameters	Control	Dex	Dex + FGF-2	Dex + PTH
Ct.Th (mm)	0.164 ± 0.004[a]	0.115 ± 0.004	0.143 ± 0.004[b,z]	0.164 ± 0.007[a,r]
MMI	0.339 ± 0.021[a]	0.186 ± 0.009	0.284 ± 0.004[b]	0.333 ± 0.036[a]

FGF-2 prevents deterioration of tibial micro-architecture in dexamethasone treated mice. Quantification of micro-CT data for various trabecular and cortical parameters of tibia is presented. Results are presented as Mean ± SEM (n = 10 mice/group). Bone volume/tissue volume (BV/TV), bone surface/tissue volume (BS/TV), trabecular separation (Tb.Sp), trabecular number (Tb.N.), structural model index (SMI), connectivity density (Conn.Dn), cross- sectional thickness (Cs.Th), mean polar moment of inertia (MMI), cross-sectional bone perimeter (B.Pm), cross-sectional tissue perimeter (T.Pm). Dex, Dexamethasone; FGF-2, Fibroblast Growth Factor-2; PTH, Parathyroid hormone.
[a] $p < 0.001$, [b] $p < 0.01$, [c] $p < 0.05$ versus Dex group.
[x] $p < 0.001$, [y] $p < 0.01$, [z] $p < 0.05$ versus Control group
[p] $p < 0.001$, [q] $p < 0.01$, [r] $p < 0.05$ versus Dex + FGF-2 group.

in femur and tibia (23% and 20% respectively; $p < 0.001$) was prevented by PTH and FGF-2 and the values were comparable to control group. The deteriorating effects of dexamethasone on micro-architectural and histomorphometric parameters are partially translated as compromised bone strength. Consistent with loss of cortical bone mass dexamethasone exhibited decreased stiffness (~51%; $p < 0.01$), energy to failure (~45% decline; $p < 0.001$) and reduced maximum load (~15%; $p < 0.001$) of femur diaphysis. FGF-2 resulted in reversal of dexamethasone induced effect on bone strength parameters, was comparable to PTH and control.

3.9. Effect of FGF-2 on bone serum markers

In line with the histological analysis the negative effects of dexamethasone on bone formation were also shown by a ~44% ($p < 0.05$) decrease of the serum bone formation marker OCN (Table 3). Moreover, serum resorption marker CTX-1 was increased in serum of dexamethasone treated animals by ~130% ($p < 0.001$). FGF-2 resulted in robust alteration in OCN level by ~173% ($p < 0.001$) and decrease of CTX-1 by 27% ($p < 0.01$). Similar results were observed in PTH group (66%). Hence, results indicated the reversal of dexamethasone induced effect on bone serum markers by FGF-2 similar to PTH.

3.10. Effect of FGF-2 on bone marrow osteoblastogenesis

We investigated whether FGF-2 treatment altered ex-vivo osteogenesis of primary bone marrow mesenchymal cells. qPCR data showed that dexamethasone suppressed the expression of transcription factor RUNX-2 ($p < 0.05$) for osteoblast differentiation and apparently formation of osteoblast cells. FGF-2 similar to PTH significantly resulted in increased RUNX-2 expression (> 2 fold change compared to control; $p < 0.01$) (Supplementary Fig. 2F) apparently maintaining the pool of osteoblast cells in bone marrow stromal cells.

3.11. FGF-2 modulated sclerostin expression in dexamethasone-treated bone tissue

Dexamethasone resulted in amplified level of sclerostin in serum (~97%; $p < 0.001$) (Table 4), while animals from FGF-2 group exhibited decline in sclerostin level (26%; $p < 0.01$) similar to PTH ($p < 0.01$), but was statistically higher ($p < 0.01$) than their control counterparts.

Immunohistochemistry displayed cells positive for sclerostin exhibited brown staining in epiphyseal trabecular regions of bone sections (Supplementary Fig. 2G). Osteocytes and matured osteoblasts in bone sections of dexamethasone group displayed intense sclerostin expression (represented by red arrow; $p < 0.01$). However, cells embedded in matrix and adjacent to trabecular network exhibited weaker sclerostin immunoreactivity compared to only dexamethasone group after FGF-2 ($p < 0.001$) and PTH ($p < 0.001$) treatment thus depicting reduced secretion of sclerostin.

3.12. Effects of FGF-2 on body weight and skeletal muscle size

Compared to control group, the body weight (Table 4) drastically declined with dexamethasone (40%; $p < 0.01$) but was unaffected with simultaneous FGF-2 and PTH treatment. Gastrocnemius and tibialis anterior (TA) muscles in the dexamethasone group exhibited sharp reduction in weight by 45% ($p < 0.01$) and 20% ($p < 0.05$), respectively. Simultaneous administration of FGF-2 counteracted glucocorticoid-induced reduction in muscle mass however, animals on PTH did not show any significant gain in muscle mass.

3.13. Effects of FGF-2 on skeletal muscle structure

Hematoxylin–eosin stain and microscopic analysis indicated that dexamethasone decreased the size of skeletal muscle cells and cause severe damage in myofibrillar architecture (Fig. 6A). The myofibrils lost

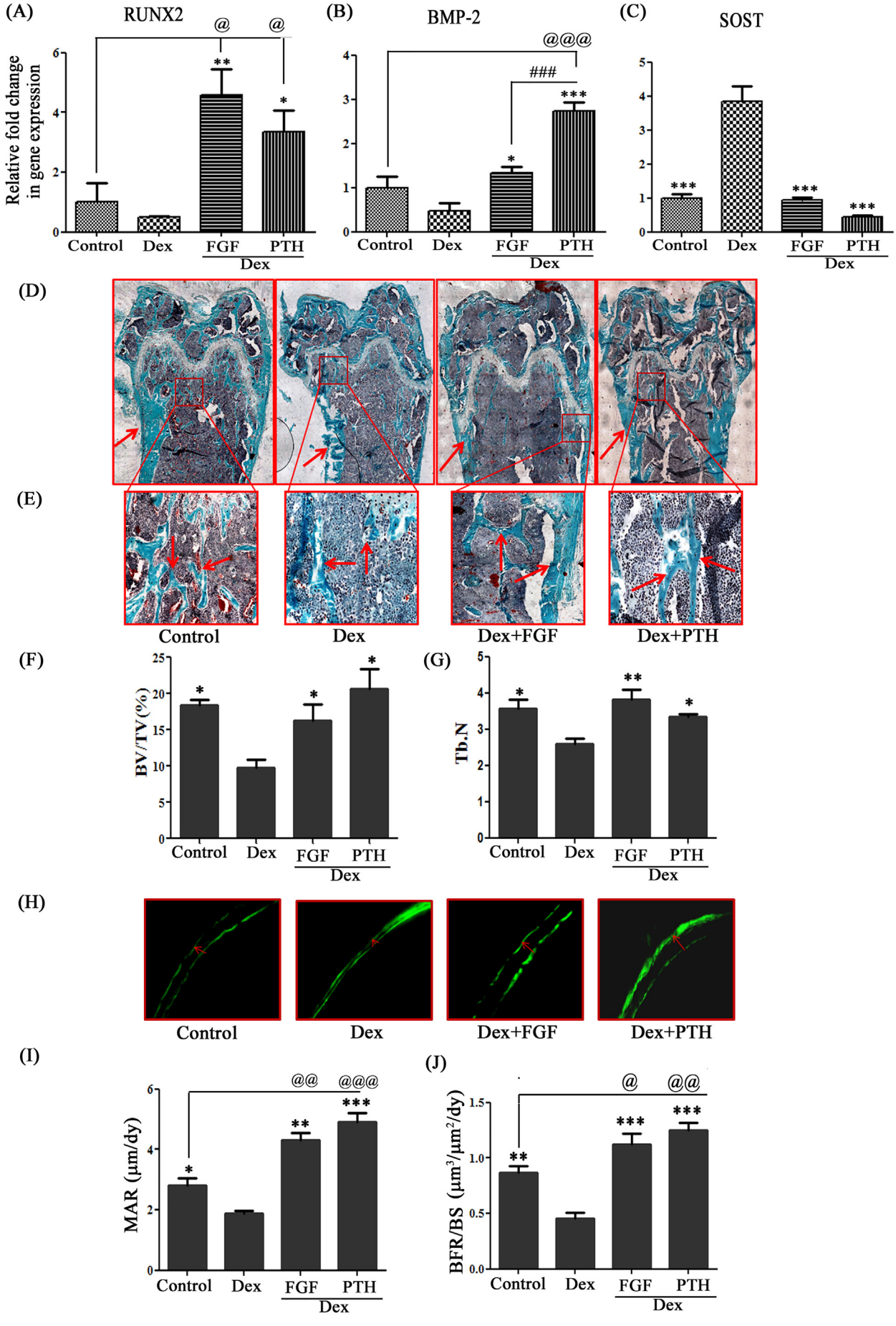

(caption on next page)

Fig. 5. FGF-2 stimulated osteogenic marker gene expression in dexamethasone induced osteoporotic animals. Quantitative PCR analysis depicting relative fold change in gene expression compared to control group are plotted in bar diagram (A) RUNX2, (B) BMP-2, (C) SOST. Data were expressed after normalization with the housekeeping gene GAPDH. (D) Representative photomicrograph (40×) of GT stained images of distal femur depicting (E) trabecular region and histomorphometric quantification using Bioquant software of (F) BV/TV %, (G) Tb.N. (H) Representative images of double fluorochrome labelling-based dynamic measures in femoral diaphyis region showing cortical changes in (I) MAR and (J) BFR/BS. Data are mean ± SEM ($n = 3$); $^{*}p < 0.05$, $^{**}p < 0.01$, $^{***}p < 0.001$ versus dex; $^{@}p < 0.05$, $^{@@}p < 0.01$ $^{@@@}p < 0.001$ versus control; $^{\#}p < 0.05$, $^{\#\#}p < 0.01$ $^{\#\#\#}p < 0.001$ versus FGF-2 + dex group. Dex, dexamethasone; FGF-2, fibroblast growth factor-2.

Table 2
Bone mineral density and bone strength.

Parameters	Control	Dex	Dex + FGF-2	Dex + PTH
Bone mineral density				
Femur ($mg.cm^{-3}$)	0.619 ± 0.045[a]	0.474 ± 0.017	0.66 ± 0.054[b]	0.6 ± 0.02[a]
Tibia ($mg.cm^{-3}$)	0.524 ± 0.034[a]	0.416 ± 0.018	0.559 ± 0.025[b]	0.511 ± 0.022[a]
Bone strength parameter				
Stiffness ($N.mm^{-1}$)	71.93 ± 5.3[b]	35.08 ± 5.18	53.95 ± 6.72[c]	55.9 ± 5.61[c]
Energy (mJ)	3.55 ± 0.4[a]	1.98 ± 0.24	3.2 ± 0.25[b]	3.1 ± 0.26[b]
Max. Power (N)	12.66 ± 0.5[a]	10.67 ± 0.6	13.5 ± 0.7[b]	12.57 ± 0.52[a]

Results are presented as Mean ± (SEM) (n = 10 mice/group).
Dex, dexamethasone; FGF-2, fibroblast growth factor-2; PTH, parathyroid hormone; BMD, bone mineral density.
[a] $p < 0.001$.
[b] $p < 0.01$.
[c] $p < 0.05$ versus dex group.

Table 3
Serum parameters.

Parameters	Control	Dex	Dex + FGF-2	Dex + PTH
SOST ($pg.ml^{-1}$)	55.84 ± 4.23[a]	110.24 ± 5.11	81.56 ± 4.38[b,y]	80.44 ± 4.96[b,y]
OCN ($ng.ml^{-1}$)	8.17 ± 0.92[c]	4.54 ± 1.07	12.4 ± 1.61[a,x]	7.56 ± 1.41[b,p]
CTX-1 ($ng.ml^{-1}$)	8.93 ± 0.97[a]	20.46 ± 3.56	14.84 ± 1.26[b,z]	6.95 ± 0.51[a,r]
Mstn ($pg.ml^{-1}$)	78.35 ± 12.35[b]	155.71 ± 10.53	91.6 ± 11.72[b]	120.43 ± 13.78[c,z]

Results are presented as Mean ± (SEM) (n = 10 mice/group).
Dex, Dexamethasone; FGF-2, Fibroblast growth factor-2; PTH, parathyroid hormone; SOST, Sclerostin; OCN, Osteocalcin; CTX-1, Carboxy-terminal collagen cross-links; Mstn, Myostatin
[a] $p < 0.001$, [b] $p < 0.01$, [c] $p < 0.05$ versus dex group.
[x] $p < 0.001$, [y] $p < 0.01$, [z] $p < 0.05$ versus Control group.
[p] $p < 0.001$, [q] $p < 0.01$, [r] $p < 0.05$ versus Dex + FGF-2 group.

Table 4
Weight of muscles after four weeks administration of FGF-2 and PTH in dexamethasone induced osteoporotic animals.

Parameters	Control	Dex	Dex + FGF-2	Dex + PTH
Gastrocnemius(mg)	116.42 ± 4.6[b]	63.7 ± 3.4	89.53 ± 3.12[b]	79.57 ± 2.88[b,q]
Tibialis anterior (mg)	46.9 ± 1.89[c]	38.0 ± 2.17	45.66 ± 2.47[c]	39.48 ± 2.17
Body weight (gms)	31.45 ± 1.56[b]	18.71 ± 2.3	28.45 ± 1.89[b]	25.45 ± 1.99[b]

Results are presented as Mean ± (SEM) (n = 10 mice/group).
Dex, Dexamethasone; FGF-2, Fibroblast growth factor-2; PTH, parathyroid hormone;
[a] $p < 0.001$, [b] $p < 0.01$, [c] $p < 0.05$ versus dex group.
[x] $p < 0.001$, [y] $p < 0.01$, [z] $p < 0.05$ versus Control group.
[p] $p < 0.001$, [q] $p < 0.01$, [r] $p < 0.05$ versus Dex + FGF-2 group.

normal form and became dwindled and overcrowded, in dexamethasone treated group (represented by arrow). It was noticeable that in several areas myofibrils were eroded away and totally disoriented. FGF-2 resulted in abrogating this deterioration induced by dexamethasone; however, no significant results were obtained in PTH group.

3.14. Effects of FGF-2 on serum myostatin and expression in muscle

Elevated serum myostatin level in dexamethasone treated group ($p < 0.01$) was prevented with concurrent treatment with FGF-2 (Table 3) as evident from values equivalent to control group. However, animals simultaneously treated with PTH displayed decreasing trend in myostatin but was significantly higher than control group.

Immunohistochemical staining of myostatin in muscle tissue showed increased ($p < 0.001$) distribution in dexamethasone animals as evident from the dark spots as compared to control (Fig. 6B). Concurrent treatment with FGF-2 exhibited reduction ($p < 0.001$) in myostatin immunoreactivity in stained muscle fibers thus displaying the preventive role of FGF-2 in dexamethasone induced muscle atrophy. Likewise, PTH too exhibited similar antagonizing effect on myostatin expression.

3.15. Effects of FGF-2 on muscle specific atrophy genes

FGF-2 exhibited a mitigating effect ($p < 0.001$) on increased

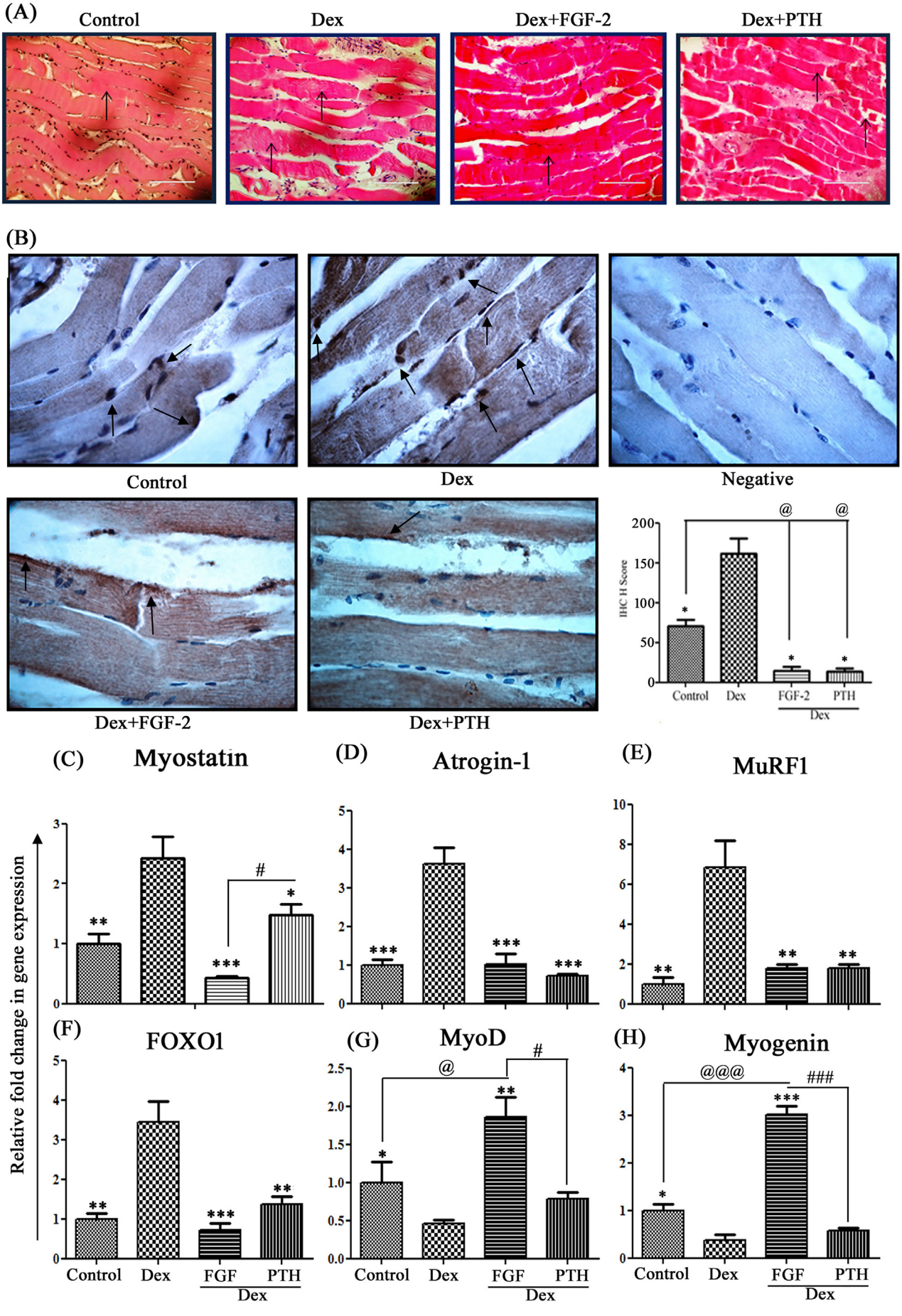

(caption on next page)

Fig. 6. (A) Representative photomicrographs of Hematoxylin-eosin stained section of muscles from treated animals showing morphological changes of skeletal muscle fibers as evident from the disoriented myofibrillar structure (arrow head) (B) Representative images of histochemical stained muscle sections for myostatin (pAb ab203076-Abcam; 1:50) in myofiber area (depicted by arrows) for various animal groups. Ten fields from each sample were analyzed according to the H-score method to represent myostatin positive cells in bar diagram. $^{*}p < 0.001$ versus dex; $^{@}p < 0.01$ versus control. Relative fold change in gene expression compared to control group was analyzed by quantitative PCR for (C) myostatin, (D) Atrogin-1, (E) MuRF-1, (F) FOXO1, (G) MyoD, and (H) Myogenin. Data are mean ± SEM (n = 3); $^{*}p < 0.05$, $^{**}p < 0.01$ $^{***}p < 0.001$ versus dex; $^{@}p < 0.05$, $^{@@}p < 0.01$ $^{@@@}p < 0.001$ versus control; $^{\#}p < 0.05$, $^{\#\#}p < 0.01$ $^{\#\#\#}p < 0.001$ versus FGF-2 + dex treated group. Dex, dexamethasone; FGF-2, fibroblast growth factor-2; PTH, parathyroid hormone 1–34.

myostatin (Fig. 6C) gene expression induced by dexamethasone. Decreased myostatin expression was associated with the down-regulation of atrophy genes atrogin-1 ($p < 0.01$) (Fig. 6D), MuRF1 ($p < 0.001$) (Fig. 6E) and FOXO1 ($p < 0.001$) (Fig. 6F), the key factors in dexamethasone-induced skeletal muscle atrophy. FGF-2 normalized the dexamethasone induced up-regulation of atrophy marker gene expression to vehicle treated control group. This further led to stimulation in MyoD ($p < 0.05$) (Fig. 6G) and myogenin ($p < 0.001$) (Fig. 6H) (~2.5 folds) expression compared to control group.

4. Discussion

Bone-muscle crosstalk involves both biomechanical and biochemical interaction of the musculoskeletal unit thus contributing to the integrity of the tissues in healthy and altered metabolic conditions [41,42]. Elevated systemic glucocorticoids, either due to underlying diseased conditions, stress, or taken exogenously for immunosuppression results in both muscle weakness and bone loss thus predisposing to an increased number of falls and fractures [43]. Experimental analyses in the current study uncovered the involvement of FGF-2 (a myokine) in antagonizing the effect glucocorticoid on musculo-skeletal deterioration. This is attributable to inhibitory effect of FGF-2 on Wnt antagonist sclerostin in bone and on myostatin a key regulator of skeletal muscle mass. Our study points out to a new aspect of FGF-2 signaling in glucocorticoid-induced degeneration of bone and muscle.

A brief treatment with FGF-2 has been reported to have a stimulatory effect on differentiation and mineralization of calvarial osteoblast cells [44]. Based on this proposition, we assessed the effect of FGF-2 on osteoblast differentiation marker protein BMP-2. FGF2 robustly stimulated the protein expression of BMP-2 by a transient treatment followed by subsequent withdrawal along with supplementation of osteogenic medium. After determination of optimum time for the treatment, we next assessed the effect of FGF-2 on dexamethasone exposed cells. In-vitro experiments on calvarial osteoblasts showed that FGF-2 could mitigate the anti-proliferative effect of dexamethasone. Moreover, inhibitory effect of dexamethasone on osteogenic marker proteins was alleviated by FGF-2 as exhibited from transcriptional analysis. Our results were in agreement with previously published reports on the effect of FGF-2 on calvarial osteoblast, wherein brief treatment with FGF-2 in early proliferation stage induced activation of certain osteogenic genes to enhance differentiation and mineralization [44,45]. Additionally, FGF-2 improved mineralization of bone marrow cells suggesting that FGF-2 was effective on osteoprogenitor cells [46,47]) as well, in presence of dexamethasone. BMP-2 and Wnt/β-catenin are the major signaling pathways inhibited by dexamethasone in osteoblast [43,48,49]. FGF-2 sustained phosphorylation of BMP-2 canonical signaling mediator Smad1/5/8, which in turn increased the expression of RUNX2 in dexamethasone treated cells. Interestingly, we also observed FGF-2 mediated inhibition of Wnt antagonist sclerostin expression which apparently led to nuclear translocation of β-catenin and thereby, antagonized the effect of dexamethasone on Wnt pathway. Overall, FGF-2 treatment abrogated dexamethasone induced inhibitory effect on osteoblasts survival pathway.

Similar to the alteration in bone signaling brought about by GC leading to bone loss, skeletal muscle development and maintenance is also impaired leading to atrophy [43]. One of the major targets of GC in inducing skeletal muscle atrophy is alteration in myostatin [30], a regulator of muscle mass [50]. As FGF-2 is one of the regulators of myostatin in skeletal muscle mass acquisition [51], we studied the effect of exogenous FGF-2 on C2C12 myoblast cell line. Dexamethasone treated C2C12 exhibited positive regulation of myostatin signaling leading to increased expression of atrogenes [18,19]. Importantly, the treatment of FGF-2 to dexamethasone exposed myotubes negatively regulated the myostatin signaling to abrogate the downstream phosphorylation of Smad 2/3 mediators. This further abridged the expression of atrogenes atrogin-1 and MuRF-1 and additionally stimulated myogenin expression to attenuate the effect of dexamethasone on differentiating muscle cells.

To determine if the observed in vitro effect was replicated in the physiological system, pharmacological dose of FGF-2 was injected in dexamethasone-induced osteoporotic animals. Concurrent treatment with FGF-2 resulted in prevention of bone loss in these animals as analyzed by bone micro-architectural parameters. Interestingly, data from FGF-2 treated animals was comparable to the other anabolic agent PTH which reverses glucocorticoid induced effects on bone [52]. Concurrent treatment of osteoporotic mice with FGF-2 increased the trabecular number and connectivity density, accompanied by reduction in trabecular separation apparently leading to improved bone volume. Indication of new bone formation was also evident from bone histomorphometry data with increased MAR and BFR. In addition to trabecular deterioration GC is capable of weakening the cortical bone as well [53]. Increased cortical thickness and periosteal of femoral diaphysis substantiated the protective effect of FGF-2 on cortical bone. Overall, improvement in cortical thickness led to increased resistance to torsional strain, which was drastically effected by dexamethasone treatment. Improved bone micro-architecture and formation rate was reflected in bone mineral density and mechanical strength parameters of FGF-2 administered animals. Volumetric BMD in FGF-2 animals were comparable to control and PTH groups. Similarly, dexamethasone induced reduction in bone stiffness, energy and power was prevented in FGF-2 treated group and was comparable to control mice. Micro–CT and bone strength data was consistent with previous data observed in ovariectomized animals on FGF-2 treatment [27] and was further substantiated by serum markers of formation and resorption. Moreover, FGF-2 also stimulated the expression of RUNX-2, BMP-2, COL-1 and OCN in vivo in dexamethasone induced osteoporotic animals thus depicting anabolic effect on osteogenesis. Additionally, the balance of RANKL and OPG expression is critical for sustaining bone formation. Dex resulted in stimulation of RANKL and down-regulation in OPG expression, consistent with previous reports [54]. FGF-2 however, mitigated the effect of dex on RANKL/OPG ratio by increasing OPG expression to facilitate osteoblastogenesis. Further, reduction in Sost and Dkk1 mRNA levels strengthened the effect of FGF-2 on Wnt/β-catenin signaling as observed in vitro. Previous reports by Hurley et.al have shown the modulation of Wnt signaling by FG-2 in mediating the anabolic action of PTH on bone formation [55,56]. Interestingly, dex induced increase in serum sclerostin level was mitigated in FGF-2 treated animals in our study. Additionally, immune-histochemical staining of femoral epiphyseal region exhibited weaker immunoreactivity for sclerostin in FGF-2 group, comparable to PTH group [57,58]. This further confirmed the effect of FGF-2 in mitigating glucocorticoid induced osteopenia by modulating sclerostin. To the best of our knowledge, this is the first example linking administration of exogenous FGF-2 to sost expression apparently leading to modulation Wnt

signaling in glucocorticoid induced osteoporotic condition.

Further, our result revealed that skeletal muscle mass was maintained in dexamethasone induced osteoporotic animals administered with FGF-2, against the sharp deterioration observed in only GC group. On investigating the underlying effect specifically on muscle tissue, it was observed that FGF-2 decreased myostatin, apparently leading to decreased atrogin-1 and MuRF1 mediated by the deactivation of FOXO1 gene expression as reported earlier [18]. This apparently led to increased expression of myoD and myogenin in skeletal muscle. Since, dexamethasone-induced muscle atrophy is associated with changes in the ultrastructure of muscle which is manifested as disorganized myofibrils [18], we assessed the histological parameter of skeletal muscles from treated animals. FGF-2 abrogated dexamethasone induced alteration in the myofibrillar architecture of skeletal muscles sections as displayed from histological data. Further, immuno-histochemical staining of skeletal muscle for myostatin revealed decreased expression in FGF-2 treated tissues thereby, establishing myostatin as a target for FGF-2 mediated antagonizing effect of glucocorticoid in skeletal muscle atrophy.

Summarizing the results obtained we suggest that the effect of FGF-2 on glucocorticoid induced bone and muscle loss is attributed to the negative regulation of sclerostin and myostatin in bone and muscle respectively. Recent reports have however pointed out to a new possibility of sclerostin expression being regulated by myostatin from muscle [59]. However, it is yet to be determined whether the changes brought about are due to FGF-2 produced in muscle, or bone or both acting in a paracrine manner. Our results are based on effect of FGF-2 on osteoporotic animals with pharmacological dose of FGF-2. Hence the scope of the present study is limited to alteration in musculoskeletal parameters based on systemic level of FGF-2.

Conclusively, our findings provide both in vitro and in vivo evidence of the effect of exogenous FGF-2 in protecting both bone and muscle loss against GC induced osteo-sarcopenia by modulating Wnt and myostatin signaling. Since, the systemic administration of FGF-2 corrected several metabolic alterations associated with adverse effect of GC on bone and muscle, it offers a unique pharmacologic opportunity to explore it from the therapeutic point of view. In future, it will also be relevant to determine whether other myokines, have similar direct effects in physiological condition where both bone and muscle are affected.

Supplementary data to this article can be found online at https://doi.org/10.1016/j.lfs.2019.05.022.

Acknowledgement

We gratefully acknowledge the University Grant Commission (UGC), Council of Scientific and Industrial Research (CSIR) (New Delhi, India), for the award of research fellowships.

References

[1] E. Canalis, G. Mazziotti, A. Giustina, J.P. Bilezikian, Glucocorticoid-induced osteoporosis: pathophysiology and therapy, Osteoporos. Int. 18 (2007) 1319–1328.
[2] D. den Uyl, I.E. Bultink, W.F. Lems, Advances in glucocorticoid-induced osteoporosis, Curr. Rheumatol. Rep. 13 (2011) 233–240.
[3] G.L. Klein, The effect of glucocorticoids on bone and muscle, Osteoporos. Sarcopenia. 1 (2015) 39–45.
[4] R.M. Pereira, J. Freire de Carvalho, Glucocorticoid-induced myopathy, Joint Bone Spine 78 (2011) 41–44.
[5] N.B. Watts, Adverse bone effects of medications used to treat non-skeletal disorders, Osteoporos. Int. 28 (2017) 2741–2746.
[6] Z. Chen, J. Xue, T. Shen, S. Mu, Q. Fu, Curcumin alleviates glucocorticoid-induced osteoporosis through the regulation of the Wnt signaling pathway, Int. J. Mol. Med. 37 (2016) 329–338.
[7] K. Ohnaka, M. Tanabe, H. Kawate, H. Nawata, R. Takayanagi, Glucocorticoid suppresses the canonical Wnt signal in cultured human osteoblasts, Biochem. Biophys. Res. Commun. 329 (2005) 177–181.
[8] W. Yao, Z. Cheng, C. Busse, A. Pham, M.C. Nakamura, N.E. Lane, Glucocorticoid excess in mice results in early activation of osteoclastogenesis and adipogenesis and prolonged suppression of osteogenesis: a longitudinal study of gene expression in bone tissue from glucocorticoid-treated mice, Arthritis Rheum. 58 (2008) 1674–1686.
[9] K. Liu, Y. Jing, W. Zhang, X. Fu, H. Zhao, X. Zhou, et al., Silencing miR-106b accelerates osteogenesis of mesenchymal stem cells and rescues against glucocorticoid-induced osteoporosis by targeting BMP2, Bone. 97 (2017) 130–138.
[10] R.C. Pereira, A.M. Delany, E. Canalis, Effects of cortisol and bone morphogenetic protein-2 on stromal cell differentiation: correlation with CCAAT-enhancer binding protein expression, Bone. 30 (2002) 685–691.
[11] N. Guanabens, L. Gifre, P. Peris, The role of Wnt signaling and sclerostin in the pathogenesis of glucocorticoid-induced osteoporosis, Curr. Osteoporos. Rep. 12 (2014) 90–97.
[12] K. Hayashi, T. Yamaguchi, S. Yano, I. Kanazawa, M. Yamauchi, M. Yamamoto, et al., BMP/Wnt antagonists are upregulated by dexamethasone in osteoblasts and reversed by alendronate and PTH: potential therapeutic targets for glucocorticoid-induced osteoporosis, Biochem. Biophys. Res. Commun. 379 (2009) 261–266.
[13] F.S. Wang, J.Y. Ko, D.W. Yeh, H.C. Ke, H.L. Wu, Modulation of Dickkopf-1 attenuates glucocorticoid induction of osteoblast apoptosis, adipocytic differentiation, and bone mass loss, Endocrinology. 149 (2008) 1793–1801.
[14] V.C. Foletta, L.J. White, A.E. Larsen, B. Leger, A.P. Russell, The role and regulation of MAFbx/atrogin-1 and MuRF1 in skeletal muscle atrophy, Pflugers Arch. 461 (2011) 325–335.
[15] O. Schakman, H. Gilson, J.P. Thissen, Mechanisms of glucocorticoid-induced myopathy, J. Endocrinol. 197 (2008) 1–10.
[16] O. Schakman, S. Kalista, C. Barbe, A. Loumaye, J.P. Thissen, Glucocorticoid-induced skeletal muscle atrophy, Int. J. Biochem. Cell Biol. 45 (2013) 2163–2172.
[17] P. Bonaldo, M. Sandri, Cellular and molecular mechanisms of muscle atrophy, Dis. Model. Mech. 6 (2013) 25–39.
[18] H. Gilson, O. Schakman, L. Combaret, P. Lause, L. Grobet, D. Attaix, et al., Myostatin gene deletion prevents glucocorticoid-induced muscle atrophy, Endocrinology. 148 (2007) 452–460.
[19] J. Rodriguez, B. Vernus, I. Chelh, I. Cassar-Malek, J.C. Gabillard, A. Hadj Sassi, et al., Myostatin and the skeletal muscle atrophy and hypertrophy signaling pathways, Cell. Mol. Life Sci. 71 (2014) 4361–4371.
[20] L. Cianferotti, M.L. Brandi, Muscle-bone interactions: basic and clinical aspects, Endocrine. 45 (2014) 165–177.
[21] M.R. Laurent, V. Dubois, F. Claessens, S.M. Verschueren, D. Vanderschueren, E. Gielen, et al., Muscle-bone interactions: from experimental models to the clinic? A critical update, Mol. Cell. Endocrinol. 432 (2016) 14–36.
[22] M.W. Hamrick, The skeletal muscle secretome: an emerging player in muscle-bone crosstalk, Bonekey Rep. 1 (2012) 60.
[23] K. Jahn, N. Lara-Castillo, L. Brotto, C.L. Mo, M.L. Johnson, M. Brotto, et al., Skeletal muscle secreted factors prevent glucocorticoid-induced osteocyte apoptosis through activation of beta-catenin, Eur. Cell. Mater. 24 (2012) 197–209 (discussion-10).
[24] Y. Kitase, J.A. Vallejo, W. Gutheil, H. Vemula, K. Jahn, J. Yi, et al., Beta-aminoisobutyric acid, l-BAIBA, is a muscle-derived osteocyte survival factor, Cell Rep. 22 (2018) 1531–1544.
[25] M.W. Hamrick, A role for myokines in muscle-bone interactions, Exerc. Sport Sci. Rev. 39 (2011) 43–47.
[26] N.E. Lane, J. Kumer, W. Yao, T. Breunig, T. Wronski, G. Modin, et al., Basic fibroblast growth factor forms new trabeculae that physically connect with pre-existing trabeculae, and this new bone is maintained with an anti-resorptive agent and enhanced with an anabolic agent in an osteopenic rat model, Osteoporos. Int. 14 (2003) 374–382.
[27] W. Yao, T. Hadi, Y. Jiang, J. Lotz, T.J. Wronski, N.E. Lane, Basic fibroblast growth factor improves trabecular bone connectivity and bone strength in the lumbar vertebral body of osteopenic rats, Osteoporos. Int. 16 (2005) 1939–1947.
[28] Y. Fei, L. Xiao, T. Doetschman, D.J. Coffin, M.M. Hurley, Fibroblast growth factor 2 stimulation of osteoblast differentiation and bone formation is mediated by modulation of the Wnt signaling pathway, J. Biol. Chem. 286 (2011) 40575–40583.
[29] L.L. Tortorella, D.J. Milasincic, P.F. Pilch, Critical proliferation-independent window for basic fibroblast growth factor repression of myogenesis via the p42/p44 MAPK signaling pathway, J. Biol. Chem. 276 (17) (2001) 13709.
[30] H.Z. Liu, Q. Li, X.Y. Yang, L. Liu, L. Liu, X.R. An, et al., Expression of basic fibroblast growth factor results in the decrease of myostatin mRNA in murine C2C12 myoblasts, Acta Biochim. Biophys. Sin. Shanghai 38 (2006) 697–703.
[31] S. Gupta, S. Adhikary, R.K. Modukuri, D. Choudhary, R. Trivedi, K.V. Sashidhara, Benzofuran-pyran hybrids: a new class of potential bone anabolic agents, Bioorg. Med. Chem. Lett. 28 (2018) 1719–1724.
[32] R. Trivedi, S. Kumar, A. Kumar, J.A. Siddiqui, G. Swarnkar, V. Gupta, et al., Kaempferol has osteogenic effect in ovariectomized adult Sprague-Dawley rats, Mol. Cell. Endocrinol. 289 (2008) 85–93.
[33] S. Adhikary, D. Choudhary, N. Ahmad, S. Kumar, K. Dev, N. Mittapelly, et al., Dried and free flowing granules of Spinacia oleracea accelerate bone regeneration and alleviate postmenopausal osteoporosis, Menopause. 24 (2017) 686–698.
[34] A. Karvande, P. Kushwaha, N. Ahmad, S. Adhikary, P. Kothari, A.K. Tripathi, et al., Glucose dependent miR-451a expression contributes to parathyroid hormone mediated osteoblast differentiation, Bone. 117 (2018) 98–115.
[35] K.J. Jepsen, M.J. Silva, D. Vashishth, X.E. Guo, M.C. van der Meulen, Establishing biomechanical mechanisms in mouse models: practical guidelines for systematically evaluating phenotypic changes in the diaphyses of long bones, J. Bone Miner. Res. 30 (2015) 951–966.
[36] S. Adhikary, D. Choudhary, N. Ahmad, A. Karvande, A. Kumar, V.T. Banala, et al., Dietary flavonoid kaempferol inhibits glucocorticoid-induced bone loss by promoting osteoblast survival, Nutrition. 53 (2018) 64–76.
[37] N. Ahmad, P. Kushwaha, A. Karvande, A.K. Tripathi, P. Kothari, S. Adhikary, et al., MicroRNA-672-5p identified during weaning reverses osteopenia and sarcopenia in

ovariectomized mice, Mol. Ther.–Nucleic Acids 14 (2019) 536–549.
[38] J. Qin, R. Du, Y.Q. Yang, H.Q. Zhang, Q. Li, L. Liu, et al., Dexamethasone-induced skeletal muscle atrophy was associated with upregulation of myostatin promoter activity, Res. Vet. Sci. 94 (2013) 84–89.
[39] G. Silvestrini, P. Ballanti, M. Leopizzi, M. Sebastiani, S. Berni, M. Di Vito, et al., Effects of intermittent parathyroid hormone (PTH) administration on SOST mRNA and protein in rat bone, J. Mol. Histol. 38 (2007) 261–269.
[40] D. Choudhary, A. Pandey, S. Adhikary, N. Ahmad, C. Bhatia, S. Bhambhani, et al., Genetically engineered flavonol enriched tomato fruit modulates chondrogenesis to increase bone length in growing animals, Sci. Rep. 6 (2016) 21668.
[41] T. Bettis, B.J. Kim, M.W. Hamrick, Impact of muscle atrophy on bone metabolism and bone strength: implications for muscle-bone crosstalk with aging and disuse, Osteoporos. Int. 29 (2018) 1713–1720.
[42] B. Guo, Z.K. Zhang, C. Liang, J. Li, J. Liu, A. Lu, et al., Molecular communication from skeletal muscle to bone: a review for muscle-derived myokines regulating bone metabolism, Calcif. Tissue Int. 100 (2017) 184–192.
[43] A.Y. Sato, M. Peacock, T. Bellido, Glucocorticoid excess in bone and muscle, Clin. Rev. Bone Miner. Metabol. 16 (2018) 33–47.
[44] A. Fakhry, C. Ratisoontorn, C. Vedhachalam, I. Salhab, E. Koyama, P. Leboy, et al., Effects of FGF-2/-9 in calvarial bone cell cultures: differentiation stage-dependent mitogenic effect, inverse regulation of BMP-2 and noggin, and enhancement of osteogenic potential, Bone. 36 (2005) 254–266.
[45] P. Li, Y. Bai, G. Yin, X. Pu, Z. Huang, X. Liao, et al., Synergistic and sequential effects of BMP-2, bFGF and VEGF on osteogenic differentiation of rat osteoblasts, J. Bone Miner. Metab. 32 (2014) 627–635.
[46] K. Hanada, J.E. Dennis, A.I. Caplan, Stimulatory effects of basic fibroblast growth factor and bone morphogenetic protein-2 on osteogenic differentiation of rat bone marrow-derived mesenchymal stem cells, J. Bone Miner. Res. 12 (1997) 1606–1614.
[47] S. Pri-Chen, S. Pitaru, F. Lokiec, N. Savion, Basic fibroblast growth factor enhances the growth and expression of the osteogenic phenotype of dexamethasone-treated human bone marrow-derived bone-like cells in culture, Bone. 23 (1998) 111–117.
[48] C.A. Luppen, R.L. Chandler, T. Noh, D.P. Mortlock, B. Frenkel, BMP-2 vs. BMP-4 expression and activity in glucocorticoid-arrested MC3T3-E1 osteoblasts: Smad signaling, not alkaline phosphatase activity, predicts rescue of mineralization, Growth Factors 26 (2008) 226–237.
[49] C.A. Luppen, E. Smith, L. Spevak, A.L. Boskey, B. Frenkel, Bone morphogenetic protein-2 restores mineralization in glucocorticoid-inhibited MC3T3-E1 osteoblast cultures, J. Bone Miner. Res. 18 (2003) 1186–1197.
[50] A. Matsakas, P. Diel, The growth factor myostatin, a key regulator in skeletal muscle growth and homeostasis, Int. J. Sports Med. 26 (2005) 83–89.
[51] H. Liu, X. An, Y. Chen, J. Zhong, Roles of extracellular signal-regulated kinase 1/2 on the suppression of myostatin gene expression induced by basic fibroblast growth factor, Acta Biochim. Biophys. Sin. Shanghai 40 (2008) 943–948.
[52] W. Yao, Z. Cheng, A. Pham, C. Busse, E.A. Zimmermann, R.O. Ritchie, et al., Glucocorticoid-induced bone loss in mice can be reversed by the actions of parathyroid hormone and risedronate on different pathways for bone formation and mineralization, Arthritis Rheum. 58 (2008) 3485–3497.
[53] M. Piemontese, J. Xiong, Y. Fujiwara, J.D. Thostenson, C.A. O'Brien, Cortical bone loss caused by glucocorticoid excess requires RANKL production by osteocytes and is associated with reduced OPG expression in mice, Am. J. Physiol. Endocrinol. Metab. 311 (2016) E587–E593.
[54] S. Thiele, N. Ziegler, E. Tsourdi, K. De Bosscher, J.P. Tuckermann, L.C. Hofbauer, et al., Selective glucocorticoid receptor modulation maintains bone mineral density in mice, J. Bone Miner. Res. 27 (2012) 2242–2250.
[55] M.G. Sabbieti, D. Agas, L. Xiao, L. Marchetti, J.D. Coffin, T. Doetschman, et al., Endogenous FGF-2 is critically important in PTH anabolic effects on bone, J. Cell. Physiol. 219 (2009) 143–151.
[56] L. Xiao, Y. Fei, M.M. Hurley, FGF2 crosstalk with Wnt signaling in mediating the anabolic action of PTH on bone formation, Bone Rep. 9 (2018) 136–144.
[57] T. Bellido, A.A. Ali, I. Gubrij, L.I. Plotkin, Q. Fu, C.A. O'Brien, et al., Chronic elevation of parathyroid hormone in mice reduces expression of sclerostin by osteocytes: a novel mechanism for hormonal control of osteoblastogenesis, Endocrinology. 146 (2005) 4577–4583.
[58] H. Keller, M. Kneissel, SOST is a target gene for PTH in bone, Bone. 37 (2005) 148–158.
[59] Y. Qin, Y. Peng, W. Zhao, J. Pan, H. Ksiezak-Reding, C. Cardozo, et al., Myostatin inhibits osteoblastic differentiation by suppressing osteocyte-derived exosomal microRNA-218: a novel mechanism in muscle-bone communication, J. Biol. Chem. 292 (2017) 11021–11033.